Journal for Geometry and Graphics
Volume 16 (2012), No. 2, 153–170.

A Flexible Planar Tessellation with a Flexion Tiling a Cylinder of Revolution*

Hellmuth Stachel

Institute of Discrete Mathematics and Geometry, Vienna University of Technology
Wiedner Hauptstr. 8–10/104, A-1230 Vienna, Austria
email: stachel@dmg.tuwien.ac.at

Abstract. Due to A. Kokotsakis a quad mesh consisting of congruent convex quadrangles of a planar tessellation is flexible. This means, when the flat quadrangles are seen as rigid bodies and only the dihedral angles along internal edges can vary, the mesh admits incongruent realizations in 3-space, so-called flexions. It has recently be proved by the author that at each nontrivial flexion all vertices lie on a cylinder of revolution. In the generic case the complete tessellation is an example of a flexible periodic framework with the property that the symmetry group of each flexion remains isomorphic to that of the initial flat pose.
The goal of this paper is to give a necessary and sufficient condition for a convex quadrangle and for the dihedral angles such that the corresponding flexion forms a tiling on a cylinder, i.e., after bending around a cylinder two boundaries of a finite mesh fit precisely together — apart from a shift. When in such a closing pose the boundaries are glued together along their overlap then the mesh is infinitesimally rigid.

Key Words: quad mesh, flexible polyhedra, periodic framework, Kokotsakis mesh, cylinder tiling, rigid origami

MSC 2010: 51M20, 52C25, 53A17, 52B70

1. Introduction

A *quadrangular mesh* ('quad mesh' by short) is a simply connected subset of a polyhedral surface with planar quadrangles as faces in the Euclidean 3-space. The edges are either *internal* when they are shared by two faces, or they belong to the boundary of the mesh.

Let the quadrangles be rigid bodies; only the dihedral angles along internal edges can vary. A quad mesh is called *continuously flexible* when there is a one-parameter set of mutually

* A preliminary version of this paper was published under the title "A flexible quadrangular mesh tiling a cylinder of revolution" in the Proceedings of the 15th International Conference on Geometry and Graphics, that took place at McGill University in Montreal, Aug. 1–5, 2012.

ISSN 1433-8157/$ 2.50

incongruent realizations of this mesh in 3-space, so-called *flexions*. The continuous movement of the mesh is called a *self-motion*.

A complete classification of all continuously flexible quad meshes is still open (compare, e.g., [2]). Open is in particular the classification of flexible 3×3 quad meshes, the so-called *Kokotsakis meshes* (see, e.g., Fig. 2), named after Antonios KOKOTSAKIS [4]. In [7] a list of five flexible types is presented. In the following we study the flexions of a very special example (cf. [4]) whose 3×3 sub-meshes are of type 5 according to this list.

2. Flexions of tessellation meshes

The following continuously flexible quad mesh dates back to A. KOKOTSAKIS [4, p. 647]. Its initial pose is flat and consists of congruent convex quadrangles of a planar tessellation. Any two quadrangles sharing an edge (like f_{ij} and $f_{i+1\,j}$ in Fig. 1) change place under a rotation through 180° (half-turn) about the midpoint of the common edge. Such a pair of adjacent quadrangles forms a centrally symmetric hexagon (see shaded area in Fig. 1). The complete tessellation can be generated by iterated translations of this hexagon. The arrows in Fig. 2 indicate the directions of these generating translations $\boldsymbol{r}$ and $\boldsymbol{l}$.

For a generic quadrangle the symmetry group of this tessellation is the wallpaper group **p2**. In the case of a deltoid the symmetry group includes also reflections and glide reflections; we obtain the wallpaper group **pmg**, when the particular case of a rhombus is excluded. An isosceles trapezoid gives rise to the group **cmm**.

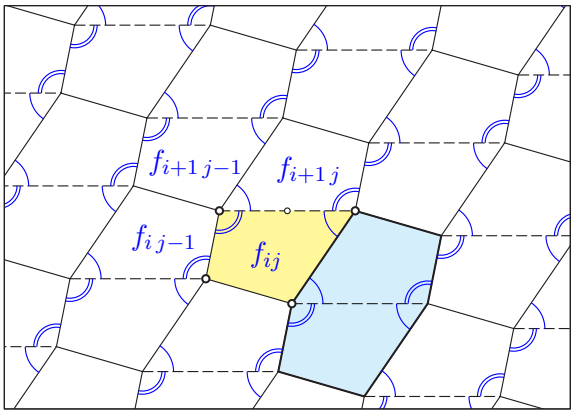

Figure 1: Kokotsakis' flexible tessellation

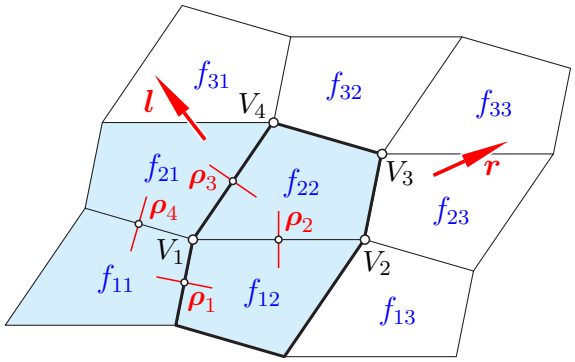

Figure 2: The mesh is generated by iterated half-turns $\boldsymbol{\rho}_1, \ldots, \boldsymbol{\rho}_4$ acting on the face f_{11}

2.1. Tessellation meshes

We recall a theorem from [9, Thm. 6, p. 12] where the flexions obtainable by a one-parameter self-motion of our planar tessellation are characterized. Additional degrees of freedom of single faces on the boundary of the mesh can be excluded by the request: Whenever the quad mesh includes three faces with a common vertex, then also the fourth face of this pyramid should be included. Thus we obtain a rectangular grid of $m \times n$ quadrangles. This is what we call an $m \times n$ *tessellation mesh* (TM for brevity).

There is a natural way to denote the quadrangles of this mesh with m rows and n columns

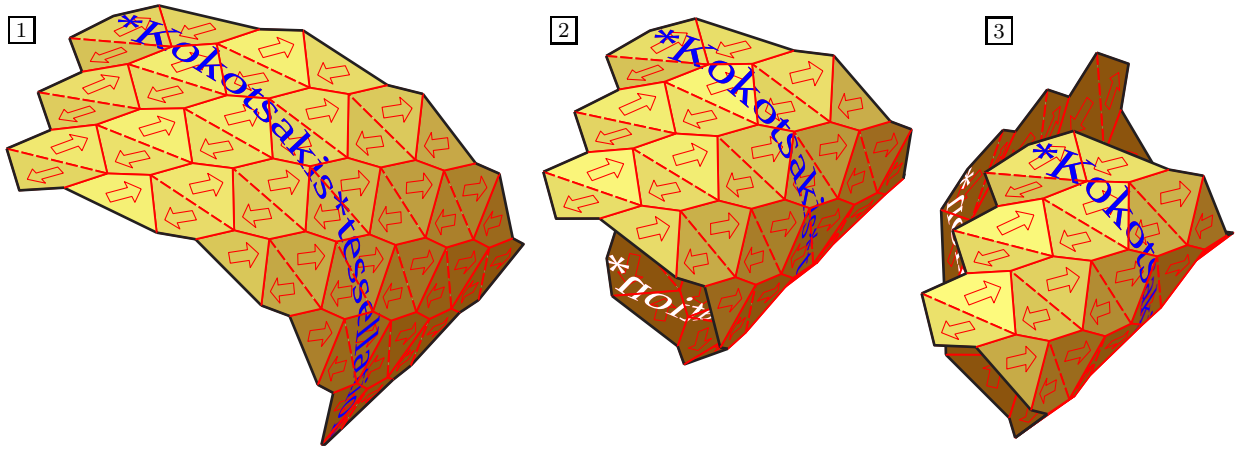

Figure 3: Three snap-shots of the self-motion of a 9×6 tessellation mesh. Dashes indicate valley folds. The text line has been affixed to emphasize the crease pattern.

by f_{ij} with $1 \le i \le m$ and $1 \le j \le n$.

$$\begin{array}{ccccc} f_{m1} & f_{m2} & f_{m3} & \cdots & f_{mn} \\ \vdots & \vdots & \vdots & & \vdots \\ f_{21} & f_{22} & f_{23} & \cdots & f_{2n} \\ f_{11} & f_{12} & f_{13} & \cdots & f_{1n} \end{array}$$

The sequences of edges between consecutive 'rows' $\{f_{ij} \,|\, j = 1, \ldots, n\}$ and $\{f_{i+1\,j} \,|\, j = 1, \ldots, n\}$, $1 \le i < m$, are called *horizontal folds*. Those between the 'columns' $\{f_{ij} \,|\, i = 1, \ldots, m\}$ and $\{f_{i\,j+1} \,|\, i = 1, \ldots, m\}$, $1 \le j < n$, form the *vertical folds* of the mesh.

By extending the 'rows' or 'columns' or both of them in both directions to infinity, we obtain respectively an $\infty \times n$ or $m \times \infty$ or $\infty \times \infty$ TM. When at the $\infty \times \infty$ mesh we fulfill the planarity constraint by erecting pyramids over the quadrangles, we obtain a periodic bar-and-joint framework (compare [3]) which admits the symmetry group **p2**.

Suppose the basic quadrangle is a *trapezoid*. Then in the flat pose the folds of one type are aligned. About each of these folds the mesh can be bended, independently from each other. We call these particular flexions *trivial*. However, the same mesh admits also nontrivial flexions (note Fig. 14), except the case with a basic parallelogram.

Theorem 1 ([9]). *All $m \times n$ tessellation meshes with convex quadrangles are flexible (Fig. 3). For $m, n \ge 3$ at each nontrivial flexion obtainable by a self-motion the vertices are located on a cylinder of revolution (see Fig. 6).*
The union of two quadrangles with a common edge is a line-symmetric hexagon. The images of this hexagon under iterated coaxial helical displacements $\boldsymbol{r}$ and $\boldsymbol{l}$ cover the complete mesh.

Proof: Here is a summary of the *proof* presented in [9]:
We start with the four faces $f_{11}, f_{12}, f_{22}, f_{21}$ sharing the vertex V_1 (shaded area in Fig. 2). These pairwise congruent faces of a 2×2 TM form a four-sided pyramid. It is flexible, provided the fundamental quadrangle is convex. Otherwise, one interior angle of a face at V_1 is greater than the sum of the other three interior angles so that the pyramid admits only the flat realization.

Step 1: Let a non-planar flexion of this pyramid be given (Fig. 4). For each pair $(f_{11}, f_{12}), \ldots, (f_{21}, f_{11})$ of adjacent faces there is a respective 180°-rotation (= *half-turn*) $\boldsymbol{\rho}_1, \ldots, \boldsymbol{\rho}_4$ which

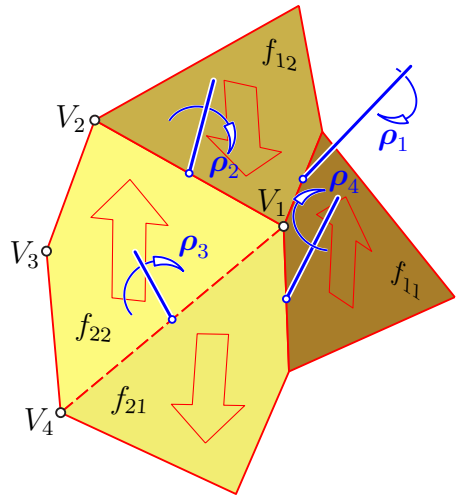

Figure 4: Flexion of a 2×2 tessellation mesh

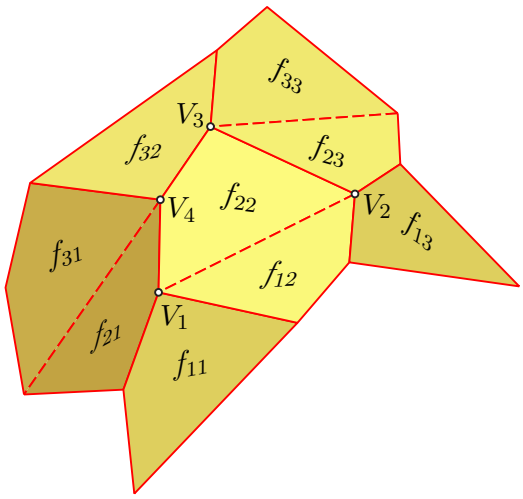

Figure 5: Flexion of a 3×3 tessellation mesh

swaps the two faces. So, e.g., $f_{12} = \boldsymbol{\rho}_1(f_{11})$ and $f_{11} = \boldsymbol{\rho}_1(f_{12})$. The axis of $\boldsymbol{\rho}_1$ is perpendicular to the common edge of f_{11} and f_{12}, and it is located in the plane which bisects the dihedral angle between f_{11} and f_{12}.

After applying the four half-turns $\boldsymbol{\rho}_1, \ldots, \boldsymbol{\rho}_4$ consecutively, the quadrangle f_{11} is mapped via f_{12}, f_{22}, and f_{21} onto itself. Hence the product $\boldsymbol{\rho}_4 \ldots \boldsymbol{\rho}_1$ equals the identity. (We indicate the composition of mappings by left multiplication.) Because of $\boldsymbol{\rho}_i^{-1} = \boldsymbol{\rho}_i$ for $i = 1, \ldots, 4$ we obtain

$$\boldsymbol{\rho}_2\boldsymbol{\rho}_1 = \boldsymbol{\rho}_3\boldsymbol{\rho}_4. \tag{1}$$

Now we recall a standard result from the geometry in 3-space: The product of two half-turns about non-parallel axes a_1, a_2 is a *helical displacement.*

- Its axis is the common perpendicular of a_1 and a_2;
- Its angle of rotation is twice the angle made by a_1 and a_2;
- Its length of translation is twice the distance between a_1 and a_2.

Note that any two coaxial helical displacements commute.

Suppose the axes of $\boldsymbol{\rho}_1$ and $\boldsymbol{\rho}_2$ are parallel (compare Fig. 4); then they were orthogonal to two adjacent edges of f_{12} and therefore orthogonal to the face f_{12}. As a consequence all four faces $f_{11}, \ldots, f_{21}$ are coplanar.

Hence conversely, when our pyramid with apex V_1 is not flat, then the axes of neighbouring half-turns cannot be parallel. Their common perpendicular is unique. Therefore (1) implies:

Lemma 2. (i) *The axes of the four half-turns* $\boldsymbol{\rho}_1, \ldots, \boldsymbol{\rho}_4$ *have a common perpendicular* p.
(ii) *At each non-flat flexion of a tessellation mesh the displacements*

$$\boldsymbol{r} := \boldsymbol{\rho}_2\boldsymbol{\rho}_1 = \boldsymbol{\rho}_3\boldsymbol{\rho}_4 \quad \textit{and} \quad \boldsymbol{l} := \boldsymbol{\rho}_4\boldsymbol{\rho}_1 = \boldsymbol{\rho}_3\boldsymbol{\rho}_2 \tag{2}$$

are helical motions with a common axis p. *Therefore they commute. In the initial flat pose* $\boldsymbol{r}$ *and* $\boldsymbol{l}$ *convert into the generating translations (see Fig. 2).*

Now we extend the flexion of the 2×2 TM (shaded area in Fig. 2) step by step to the complete $m \times n$ mesh by adding congruent copies of the initial pyramid without restricting the flexibility. First we concentrate on the 3×3 mesh displayed in Fig. 2:

Step 2: The half-turn $\boldsymbol{\rho}_2$ exchanges not only f_{12} with f_{22} but maps the pyramid with apex V_1 onto a congruent copy with apex V_2 sharing two faces with its preimage. We get $f_{13} = \boldsymbol{\rho}_2(f_{21})$ and $f_{23} = \boldsymbol{\rho}_2(f_{11})$. Analogously, $\boldsymbol{\rho}_3$ generates a pyramid with apex V_4 which shares the two faces f_{22} and f_{21} with the initial pyramid, and $f_{31} = \boldsymbol{\rho}_3(f_{12})$, $f_{32} = \boldsymbol{\rho}_3(f_{11})$.

Finally there are two ways to generate a pyramid with apex V_3. Either, we transform $\boldsymbol{\rho}_1$ by $\boldsymbol{\rho}_2$ and apply $\boldsymbol{\rho}_2\boldsymbol{\rho}_1\boldsymbol{\rho}_2$, which exchanges f_{22} with f_{23} and swaps V_2 and V_3. Or we proceed with $\boldsymbol{\rho}_3\boldsymbol{\rho}_4\boldsymbol{\rho}_3$, which exchanges f_{22} with f_{32} and swaps V_4 and V_3.

Thus we obtain mappings $(\boldsymbol{\rho}_2\boldsymbol{\rho}_1\boldsymbol{\rho}_2)\boldsymbol{\rho}_2 = \boldsymbol{\rho}_2\boldsymbol{\rho}_1$ and $(\boldsymbol{\rho}_3\boldsymbol{\rho}_4\boldsymbol{\rho}_3)\boldsymbol{\rho}_3 = \boldsymbol{\rho}_3\boldsymbol{\rho}_4$ with $V_1 \mapsto V_3$. Both displacements are equal by (1), and we notice

$$\boldsymbol{r} = \boldsymbol{\rho}_2\boldsymbol{\rho}_1 = \boldsymbol{\rho}_3\boldsymbol{\rho}_4 \colon\ V_1 \mapsto V_3,\ f_{11} \mapsto f_{22},\ f_{12} \mapsto f_{23},\ f_{21} \mapsto f_{32},\ f_{22} \mapsto f_{33}. \tag{3}$$

Hence each flexion of the initial pyramid with apex V_1 is compatible with a flexion of the 3×3 TM displayed in Figs. 2 or 5. It is proved in [9, Lemma 8] that this the only way to extend the given flexion of the 2×2 TM, provided we restrict to flexions obtainable by a self-motion from the initial flat pose.[1]

According to Lemma 2 the helical displacements $\boldsymbol{r} = \boldsymbol{\rho}_2\boldsymbol{\rho}_1$ and $\boldsymbol{l} = \boldsymbol{\rho}_4\boldsymbol{\rho}_1 = \boldsymbol{\rho}_3\boldsymbol{\rho}_2$ are the spatial analogues of the generating translations in the plane. $\boldsymbol{r}$ maps V_1 onto V_3, and $\boldsymbol{l}$ maps the pyramid with apex V_2 onto that with apex V_4. Thus we have

$$\boldsymbol{l} = \boldsymbol{\rho}_4\boldsymbol{\rho}_1 = \boldsymbol{\rho}_3\boldsymbol{\rho}_2 \colon\ V_2 \mapsto V_4,\ f_{12} \mapsto f_{21},\ f_{13} \mapsto f_{22},\ f_{22} \mapsto f_{31},\ f_{23} \mapsto f_{32}. \tag{4}$$

Step 3: Finally, we continue this flexion of the 3×3 mesh to the complete $m \times n$ TM: From Eqs. (3) and (4) we conclude that $\boldsymbol{l}^{-1}\boldsymbol{r} = \boldsymbol{r}\boldsymbol{l}^{-1}$ acts like a horizontal shift and maps the left column (f_{11}, f_{21}, f_{31}) onto the right column (f_{13}, f_{23}, f_{33}) of our 3×3 TM. When $\boldsymbol{l}^{-1}\boldsymbol{r}$ acts on the complete 3×3 mesh, we get a second mesh which shares with the original one the column (f_{13}, f_{23}, f_{33}); the union is a 5×3 mesh. This can be iterated; $(\boldsymbol{l}^{-1}\boldsymbol{r})^2 = \boldsymbol{l}^{-2}\boldsymbol{r}^2$ extends by two more columns, and so on. After k extensions we end up with a $(2k+3) \times 3$ mesh.

On the other hand the vertical shift $\boldsymbol{l}\boldsymbol{r} = \boldsymbol{r}\boldsymbol{l}$ maps the row (f_{11}, f_{12}, f_{13}) onto the third row (f_{31}, f_{32}, f_{33}). Since this vertical shift commutes with the horizontal one, the same holds for our $(2k+3) \times 3$ mesh. The same procedure as before allows to extend our flexion stepwise upwards by pairs of rows. Hence after l extensions we obtain a flexion of a $(2k+3) \times (2l+3)$ TM. Due to [9, Lemma 8] for each added 3×3 mesh the flexion is unique when we restrict to nontrivial flexions which can be reached during a (continous) self-motion.

All vertices of this flexion arise from V_1 by displacements which keep the common perpendicular p of the half-turns' axes fixed. For example, according to Fig. 2

$$V_2 = \boldsymbol{\rho}_2(V_1),\ V_3 = \boldsymbol{r}(V_1),\ V_4 = \boldsymbol{\rho}_3(V_1). \tag{5}$$

This is the reason why all vertices have the same distance to p. Hence they are located on a cylinder of revolution with axis p (note the cylinder in Fig. 6).

When f_{12} and f_{22} are glued together, we obtain a skew hexagon, one half of our initial pyramid with apex V_1 (see Fig. 2). The half-turn $\boldsymbol{\rho}_2$ maps this hexagon onto itself; hence it is line-symmetric. By (3) the helical displacement $\boldsymbol{r}$ maps this hexagon onto the compound of f_{23} and f_{33}. The displacement $\boldsymbol{l}$ maps the compound of f_{12} and f_{22} onto f_{21} and f_{31}. When

[1] According to [9] under particular conditions also other flexions are possible, but they are isolated.

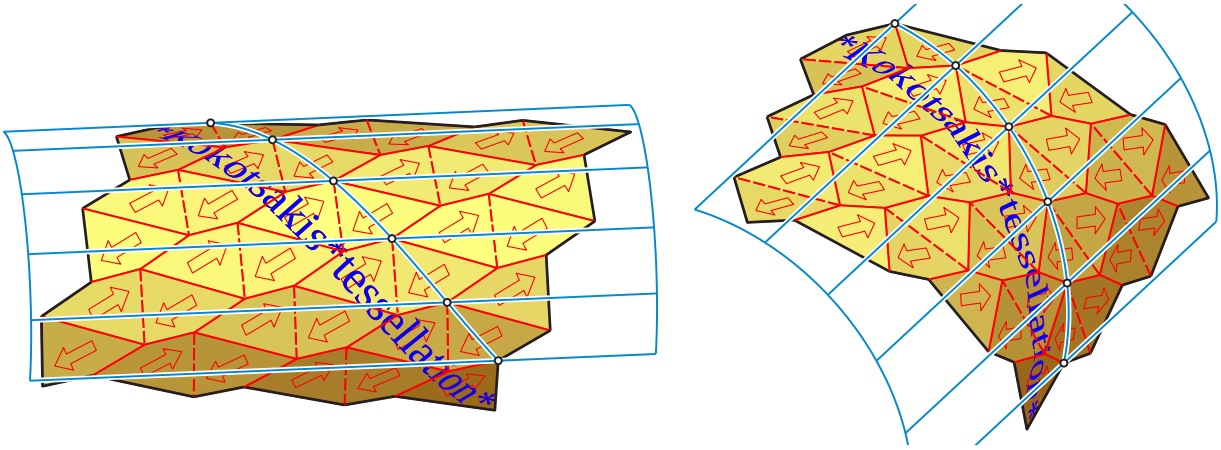

Figure 6: At each flexion of the first or second kind all vertices are placed on a cylinder of revolution; the marked vertices can be joined by a helical line.

these two helical displacements act repeatedly on the line-symmetric hexagon, the complete flexion is obtained. This completes the main arguments for Theorem 1. □

According to [9, Remark 2] the flat pose admits a bifurcation between two analytic self-motions of the TM. Figure 6 shows flexions of different kinds of a 6×6 TM.

2.2. Computation of flexions

How to compute a flexion? According to Fig. 7 the interior angles $(\delta, \alpha, \gamma, \beta)$ of the faces define the consecutive side lengths of the *spherical four-bar* which controls the dihedral angles of the (flexible) 2×2 mesh. The related formulas can be found in [7, (1) – (6)]. Figure 7 (b) reveals that for given dihedral angle φ_1 along the edge V_1V_2 there exist two corresponding points B and $\overline{B}$ at the spherical four-bar and therefore two flexions of the TM.

In the initial pose the corresponding spherical four-bar constitutes a great circle. The statement Lemma 2 (i) is equivalent to the claim that at non-folded poses the exterior bisectors of the spherical quadrangle A_0ABB_0 share a pair of antipodal points. Corresponding to the

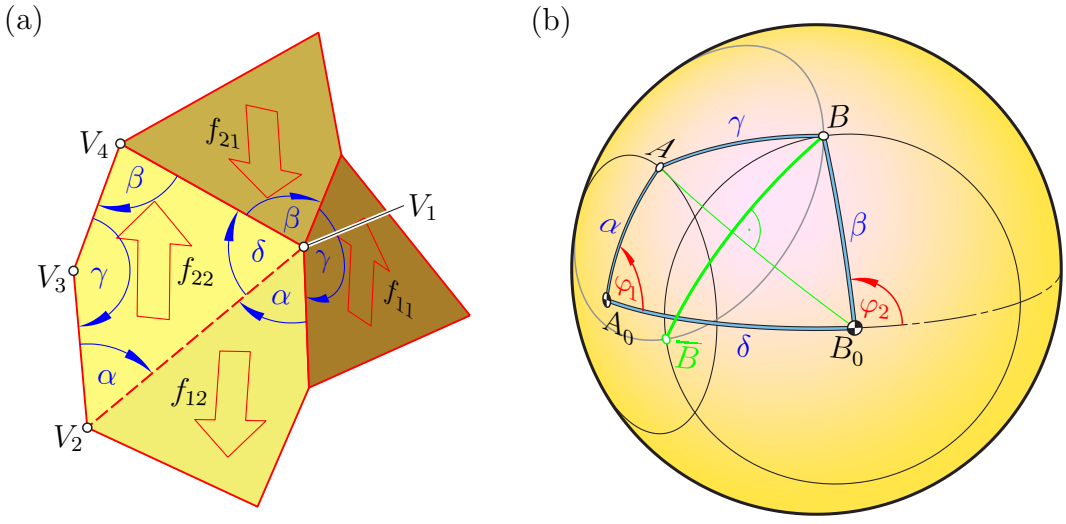

Figure 7: The interior angles in the flat quadrangle serve as side lengths of the spherical four-bar A_0ABB_0 which controls the dihedral angles of the flexion

trivial flexions (note page 155) in the trapezoidal case, e.g., $\alpha+\gamma=\delta+\beta=\pi$, point B stays fixed opposite to A_0 and the half-circle from A_0 via A to B rotates about the axis A_0B.

After extending our 2×2 mesh to an $m\times n$ TM self-intersections can occur. But they can even show up at our initial pyramid as soon as the spherical quadrangle has a self-intersection.

There is a second way to compute the flexions (see Fig. 8): The plane $[f_{22}]$ spanned by the convex quadrangle $V_1\dots V_4$ of f_{22} intersects the circumcylinder of the flexion (Theorem 1) along an ellipse e. There is a *pencil of conics* passing through the four vertices V_1, …, V_4. Hence we can choose any ellipse from this pencil and specify one of the two cylinders of revolution passing through this ellipse. Now we define the half-turns $\boldsymbol{\rho}_2$ and $\boldsymbol{\rho}_3$: Their axes pass through the midpoints of the sides V_1V_2 and V_1V_4, respectively, and intersect the cylinder's axis p perpendicularily (compare Fig. 4). The common normal between V_2V_3 and p is the axis of $\boldsymbol{\rho}_2\boldsymbol{\rho}_1\boldsymbol{\rho}_2$, that between V_3V_4 and p is the axis of $\boldsymbol{\rho}_3\boldsymbol{\rho}_4\boldsymbol{\rho}_3$. Interations of these half-turns transform our initial face f_{22} into all faces of the flexion.

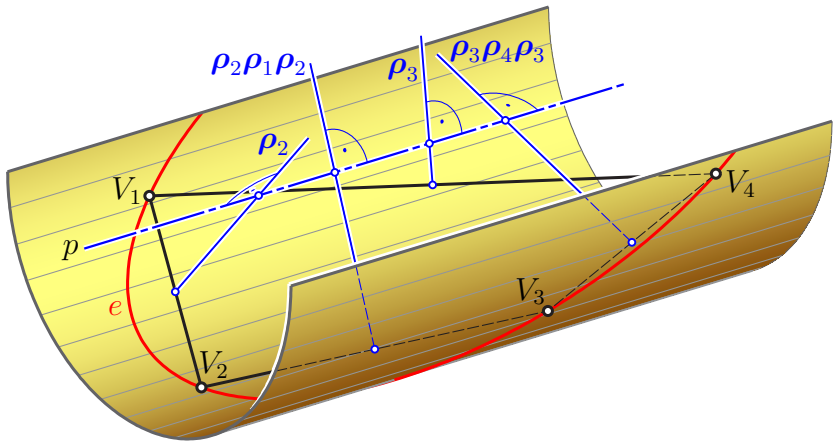

Figure 8: Each ellipse e through the planar quadrangle $V_1\dots V_4$ defines a non-flat flexion of the tessellation mesh

It is wellknown from Projective Geometry that the centers of conics passing through the vertices $V_1\dots V_4$ of a quadrangle are placed on a conic, the *nine-point conic* of the quadrangle. It contains the midpoints of the sides and diagonals and the vertices of the diagonal triangle. For a convex quadrangle different from a trapezoid the center curve is a hyperbola, and one branch is reserved for the centers of ellipses included in the pencil (see [5, p. 411]).

Due to [5, p. 409] the axes of the cylinders are parallel to the generators of an orthogonal quadratic cone which intersects the spanned plane in two real lines parallel to the axes of parabolas passing through $V_1\dots V_4$. In the generic case the ruled surface swept by the cylinder axes is algebraic of degree 8.

Corollary 3. *For a given tessellation mesh the cylinders of revolution addressed in Theorem 1 have the following properties:*

(i) *Their axes intersect the affine span of any face f_{jk} of the mesh along one branch of a hyperbola, the nine-point conic of the included quadrangle. Only in the case of a trapezoid or parallelogram the hyperbola splits into two lines.*

(ii) *Relative to f_{jk} the axes are parallel to generators of an orthogonal quadratic cone, which has a symmetry plane parallel to $[f_{jk}]$. This director cone splits into planes if and only if the basic quadrangle $V_1\dots V_4$ has a circumcircle. Then these two planes are orthogonal.*

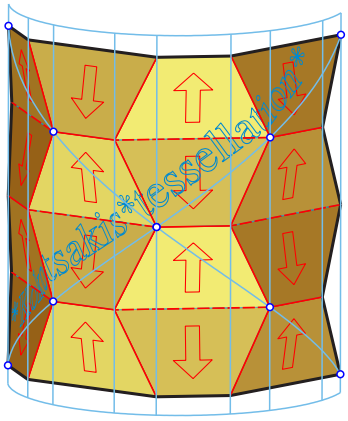

Figure 9: In the case of a symmetric trapezoid the nontrivial flexion has planes of symmetry

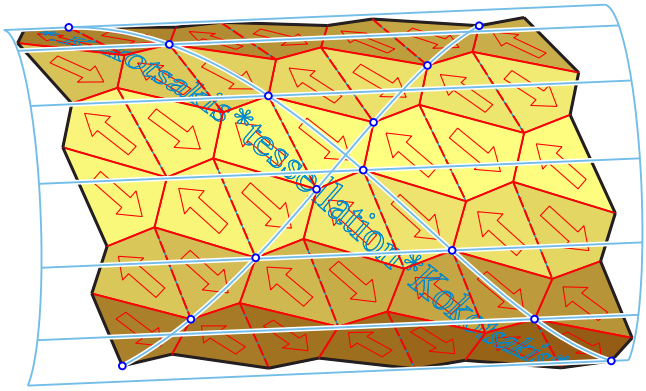

Figure 10: The axial or planar symmetries of a deltoid as basic quadrangle cannot be extended to local symmetries of non-flat flexions

2.3. Particular cases

In this subsection we study the particular cases where the basic convex quadrangle is either a trapezoid, a deltoid or a cyclic quadrangle, i.e., a quadrangle with circumcircle.

Theorem 4. (i) *When the quadrangles of the tessellation mesh are trapezoids (note Fig. 14), then at each nontrivial flexion either* $\boldsymbol{lr}$ *or* $\boldsymbol{l}^{-1}\boldsymbol{r}$ *is a translation along* p.
(ii) *For a symmetric trapezoid all nontrivial flexions admit locally planar reflections.*[2]

Proof: According to the proof of Lemma 2 the axis p of the cylinder is the common perpendicular of all axes of half-rotations which exchange pairs of neighbouring faces $(f_{ij}, f_{i+1\,j})$ or $(f_{ij}, f_{i\,j+1})$. For each internal edge e_k of a flexion there exists a half-rotation $\boldsymbol{\rho}_k$ mapping e_k onto itself. The axis of $\boldsymbol{\rho}_k$ is orthogonal to e_k (see Fig. 4).

(i) Let f_{11} be a trapezoid with parallel edges e_1 and e_2. There are two cases to distinguish:

- When the axes of the half-rotations corresponding to e_1 and e_2 are not parallel, then their common perpendicular p is unique and necessarily parallel to e_1 and e_2. This implies, that the images of e_1 and e_2 under all helical motions about p are parallel to p. The folds of one type are aligned; the flexion is trivial in the sense mentioned above on page 155.
- When the axes of the half-rotations corresponding to e_1 and e_2 are parallel then the product of these half-rotations is a translation, which maps the neighbour face of f_{11} along e_1 onto the neighbour face along the opposite side e_2.

(ii) Now the quadrangle $V_1 \dots V_4$ in Fig. 4 is a symmetric (or isosceles) trapezoid f_{22} with parallel sides $e_1 = V_1V_4$ and $e_2 = V_2V_3$. Then the reflection in the plane of symmetry of the pair (V_1, V_4) (and at the same time of (V_2, V_3)) maps the trapezoid onto itself. Its product with $\boldsymbol{\rho}_3$ is a planar reflection $\boldsymbol{\sigma}_{14}$ which interchanges f_{22} and its neighbor face f_{21}. The plane of reflection is spanned by the common edge $e_1 = V_1V_4$ and by the axis of $\boldsymbol{\rho}_3$. There is also a planar reflection $\boldsymbol{\sigma}_{23}$ interchanging the faces f_{22} and f_{23} through the opposite edge $e_2 = V_2V_3$. The reflecting planes of $\boldsymbol{\sigma}_{14}$ and $\boldsymbol{\sigma}_{23}$ must be parallel since the edges e_1, e_2 are parallel as

[2] *'Local'* means that for a finite TM the symmetry works only in a sufficiently small neighborhood of the face but need not map the boundary onto itself.

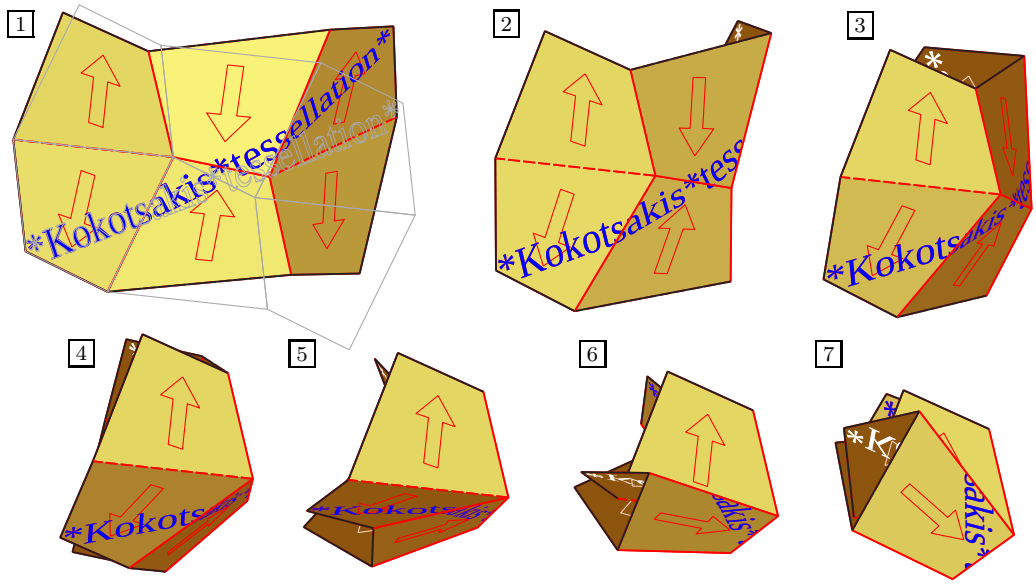

Figure 11: For particular quadrangles with a circumcircle a 3×2 tessellation mesh can continuously be folded without self-intersections so that finally it can be 'packed' into the interior of one single circumcircle

well as the axes of the corresponding axes — due to the first part of this proof. The product $\boldsymbol{\sigma}_{23}\,\boldsymbol{\sigma}_{14}$ of these reflections is a translation mapping f_{21} onto f_{23}. Due to statement (a) this is a translation along the cylinder axis p. Therefore the reflecting planes of $\boldsymbol{\sigma}_{14}$ and $\boldsymbol{\sigma}_{23}$ of the planar reflections are orthogonal to p and the same holds for the included parallel edges e_1, e_2 of the symmetric trapezoid (note Fig. 9). □

Figure 10 reveals that in the case of a *deltoid* the axis of symmetry of a single deltoid is not orthogonal to the axis of the circumscribed cylinder, and the plane of symmetry of the deltoid does not pass through the cylinder axis p. Hence, neither the half-turn nor the planar reflection which maps a single face onto itself gives a local symmetry operation of the non-flat flexion of the TM.

When the quadrangle in Fig. 8 has a *circumcircle*, then among the ellipses through the vertices there is a circle with only one cylinder of rotation passing through. In this case the axes of half-turns $\boldsymbol{\rho}_1, \ldots, \boldsymbol{\rho}_4$ are all coplanar. The complete flexion is flat; the circumcircles of all faces coincide. Similar to Miura-ori (see, e.g., [8]) this TM can be 'packed' into very small size such that it finds place in the circumcircle of one quadrangle — at least 'theoretically', i.e., without paying attention to self-intersections. Since opposite angles in the convex quadrangle $V_1 \ldots V_4$ are complementary (compare Fig. 7), the included 3×3 Kokotsakis meshes are of isogonal type ([7, type III]), while at the same time all 3×3 TMs are particular examples of the line-symmetric type V ([7, p. 436]).

However, we can state that such a flat folded pose cannot be obtained with a physical 3×3 TM without self-intersections — except the case with a square $V_1 \ldots V_4$. Only a 3×2 TM can admit a self-movement without collisions between the unfolded initial pose and the completely folded second flat pose in the interior of one single circumcircle (see series of snapshots in Fig. 11).[3]

[3]Under the assumption $\beta < \gamma < \delta < \alpha$ a sufficient condition for an intersection-free folded flat pose is

2.4. Symmetry group of flexions

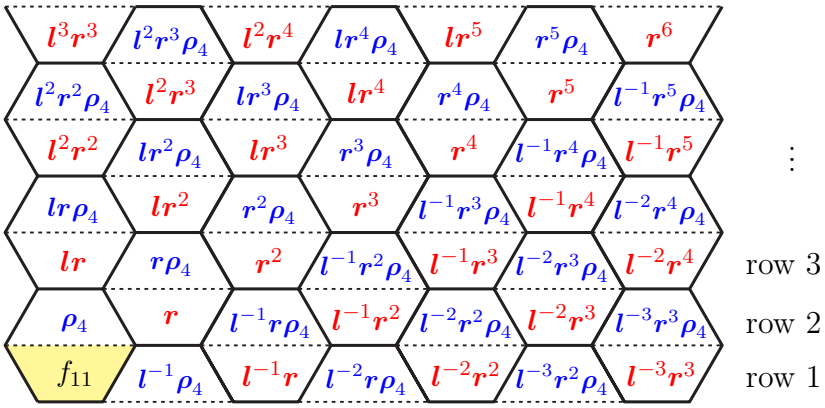

Figure 12: This table shows the images of f_{11} under the indicated transformations for a 7×7 tessellation mesh

We recall from the proof of Theorem 1 that for any nontrivial flexion of an $m \times n$ TM the helical displacements $\boldsymbol{r}$, $\boldsymbol{l}$ and the half-turn $\boldsymbol{\rho}_4$ are local symmetry operations. This holds for arbitrarily large (m, n), hence also for the $\infty \times \infty$ mesh. According to Eqs. (3) and (4) we have

$$\boldsymbol{r}\colon\ f_{ij} \mapsto f_{i+1\,j+1}, \quad \boldsymbol{l}\colon\ f_{ij} \mapsto f_{i+1\,j-1}. \tag{6}$$

The scheme in Fig. 12 shows which transformations must be applied to the face f_{11} to cover the faces of the displayed 7×7 TM. These orientation-preserving displacements are unique provided the quadrangle itself does not admit an axial symmetry.[4] Hence, after applying $\boldsymbol{r}^x$ and $\boldsymbol{l}^y$ on the face f_{11}, we obtain f_{ij} with

$$\begin{pmatrix} i \\ j \end{pmatrix} = \begin{pmatrix} 1 \\ 1 \end{pmatrix} + x \begin{pmatrix} 1 \\ 1 \end{pmatrix} + y \begin{pmatrix} 1 \\ -1 \end{pmatrix} = \begin{pmatrix} 1+x+y \\ 1+x-y \end{pmatrix}$$

with $i+j = 2(1+x) \equiv 0 \pmod 2$. For given i, j with an even sum we can solve these equations for x and y which yields an unique result. For odd $i + j$ at first $\boldsymbol{\rho}_4$ has to be applied to f_{11}. We summarize:

Lemma 5. *At each nontrivial flexion of an $m \times n$ tessellation mesh the face f_{11} can be mapped onto the face f_{ij} according to the following rule:*

$$f_{ij} = \begin{cases} \boldsymbol{l}^{\frac{i-j}{2}} \boldsymbol{r}^{\frac{i+j}{2}-1}(f_{11}) & \text{for } i+j \equiv 0 \pmod 2, \\ \boldsymbol{l}^{\frac{i-j-1}{2}} \boldsymbol{r}^{\frac{i+j-3}{2}} \boldsymbol{\rho}_4(f_{11}) & \text{for } i+j \equiv 1 \pmod 2. \end{cases}$$

From (6) we obtain for the shifts along 'rows' and 'columns'

$$\boldsymbol{lr} = \boldsymbol{rl}\colon f_{ij} \mapsto f_{i+2\,j}, \quad \boldsymbol{l}^{-1}\boldsymbol{r} = \boldsymbol{r}\boldsymbol{l}^{-1}\colon f_{ij} \mapsto f_{i\,j+2},$$

$\beta < \sphericalangle V_4V_1V_3$. Then the faces can be placed one upon the other in the order $f_{22}, f_{21}, f_{11}, f_{23}, f_{13}, f_{12}$. If this mesh is extended by a third row to a 3×3 TM then this sequence must start under f_{22} either with f_{31}, f_{32}, f_{33} or with f_{32}, f_{31}, f_{33}. However, there is not enough space, neither for f_{32} between f_{31} and f_{33} nor for f_{31} between f_{32} and f_{33}.

[4]The uniqueness of the displacement does not imply that its decomposition into a product of $\boldsymbol{r}$, $\boldsymbol{l}$ and $\boldsymbol{\rho}_4$ is unique, too. We find counterexamples in the case of horizontally closing flexions (Theorem 7).

and furthermore

$$\boldsymbol{\rho}_4 \colon f_{ij} \mapsto f_{3-i\,2-j}. \tag{7}$$

The group generated by $\boldsymbol{l}$, $\boldsymbol{r}$ and $\boldsymbol{\rho}_4$ acts sharply transitive on the faces of the flexion. This follows from the fact that due to

$$\boldsymbol{l}\boldsymbol{r} = \boldsymbol{r}\boldsymbol{l}, \quad \boldsymbol{\rho}_4^{-1} = \boldsymbol{\rho}_4, \quad \boldsymbol{\rho}_4\boldsymbol{l}\boldsymbol{\rho}_4 = \boldsymbol{l}^{-1} \text{ and } \boldsymbol{\rho}_4\boldsymbol{r}\boldsymbol{\rho}_4 = \boldsymbol{r}^{-1}$$

each product of $\boldsymbol{l}$, $\boldsymbol{r}$ and $\boldsymbol{\rho}_4$ can be rewritten as $\boldsymbol{l}^x\boldsymbol{r}^y$ or as $\boldsymbol{l}^x\boldsymbol{r}^y\boldsymbol{\rho}_4$. Therefore in the case of a non-flat flexion the group generated by $\boldsymbol{l}$, $\boldsymbol{r}$ and $\boldsymbol{\rho}_4$ is isomorphic to that of the initial flat pose. This can also be concluded more explicitely from the representations of $\boldsymbol{l}$, $\boldsymbol{r}$ and $\boldsymbol{\rho}_4$ in cylinder coordinates by (9) in the next section or from an unfolding of the circumference cylinder.

In Section 2.3 we learned that only in the case of a symmetric trapezoid (Fig. 9) the non-flat flexions admits additional symmetry operations. This results in

Theorem 6. *All poses obtained by nontrivial self-motions of an $\infty \times \infty$ tessellation mesh are periodic. The group of symmetries of the immersed flexion*[5] *is isomorphic to the wallpaper group* **p2** *except in the case of a symmetric trapezoid where the symmetry group includes also planar reflections and is isomorphic to* **cmm**.

3. Horizontally closing flexions of tessellation meshes

3.1. Closure conditions

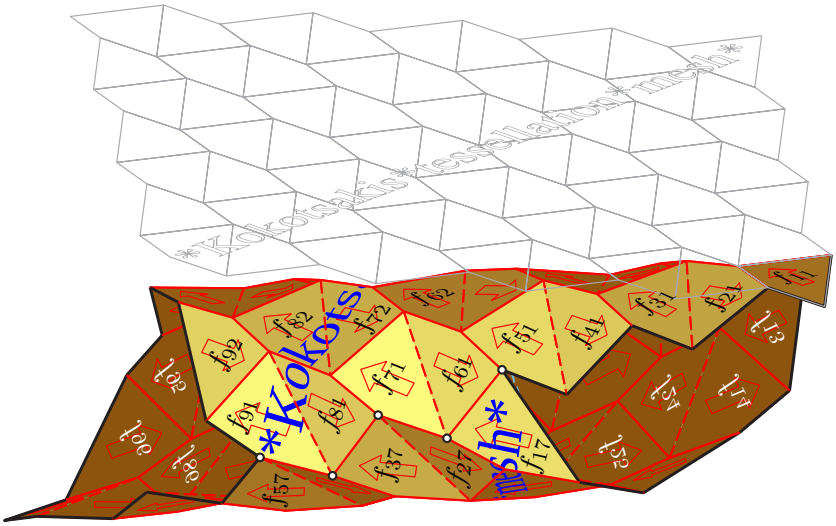

Figure 13: A flexion of a 9×7 tessellation mesh which closes horizontally with shift $k = 5$. The flat initial pose is shown in gray color.

Suppose, a particular non-trivial flexion of an $m \times n$ tessellation has the property that after surrounding the circumscribed cylinder the right border fits exactly to the left border of the mesh — apart from a vertical shift by k faces (Fig. 13). Then we call this flexion *horizontally*

[5] When the flexion closes in the sense of Theorem 7, then the symmetry group of the *embedded* flexion, i.e., of a cylinder tessellation, changes because then a product $\boldsymbol{l}^a\boldsymbol{r}^b$ with $a, b \in \mathbb{Z}$ equals the identity.

closing. Of course, also a *vertically closing* flexion is possible when the upper border fits exactly to the lower border. However, by interchanging rows with columns this case can be reduced to the previous one.

Let a horizontally closing flexion of our $m \times n$ mesh with a vertical shift of k faces be given.[6] Then there are two cases to distinguish:

- For *odd* n the face $f_{2\,n+1} = \boldsymbol{r}(f_{1n})$ must be identical with the face $f_{k+2\,1}$ of the most-left row, $k \equiv 1 \pmod 2$. Lemma 5 implies

$$\boldsymbol{l}^{\frac{1-n}{2}}\boldsymbol{r}^{\frac{n+1}{2}} = \boldsymbol{l}^{\frac{k+1}{2}}\boldsymbol{r}^{\frac{k+1}{2}}\,\boldsymbol{t}_{2\pi}$$

  where $\boldsymbol{t}_{2\pi}$ stands for a full turn, i.e., a rotation about the axis p through 2π. Since the involved coaxial helical motions commute, we obtain

$$\boldsymbol{l}^{-\frac{n+k}{2}}\boldsymbol{r}^{\frac{n-k}{2}} = \boldsymbol{t}_{2\pi}. \tag{8}$$

- *n even*: Now in the case of an exact fit $f_{1\,n+1}$ equals $f_{k+1\,1}$ with $k \equiv 0 \pmod 2$, which means by Lemma 5

$$\boldsymbol{l}^{-\frac{n}{2}}\boldsymbol{r}^{\frac{n}{2}} = \boldsymbol{l}^{\frac{k}{2}}\boldsymbol{r}^{\frac{k}{2}}\,\boldsymbol{t}_{2\pi}.$$

  This is again equivalent to (8).

Note $k \equiv n \pmod 2$. We substitute $a = -\dfrac{n+k}{2}$ and $b = \dfrac{n-k}{2}$ and summarize:

Theorem 7. *A non-trivial flexion of the $m \times n$ tessellation mesh is horizontally closing, i.e., after surrounding the circumscribed cylinder the right border zig-zag fits exactly to the left border zig-zag under a vertical shift of k faces, if and only if there are integers $a, b \in \mathbb{Z}$ with*

$$n = -a + b\,,^{7} \quad k = -a - b \quad \textit{and} \quad \boldsymbol{l}^a\boldsymbol{r}^b = \boldsymbol{t}_{2\pi}$$

where $\boldsymbol{t}_{2\pi}$ denotes the full rotation about the cylinder axis p. A band with $|a+b|$ rows, i.e., an $\infty \times |a+b|$ tessellation mesh based on the same quadrangle has a flexion in form of a simply covered cylinder tessellation (note, e.g., Fig. 16). The extension of our horizontally closing flexion to an $\infty \times \infty$ mesh has the property $f_{i\,j+n} = f_{i+k\,j}$.

3.2. First examples

The following two examples of horizontally closing flexions have been found numerically: The dimensions of the quadrangle and the bending angles were varied such that after surrounding the cylinder one vertex of the right border line converges against an appropriate vertex of the left border line.

Example 1. At the example depicted in Fig. 13 we have $n = 7$ and $k = 5$ and therefore by (8) $\boldsymbol{l}^{-6}\boldsymbol{r} = \boldsymbol{t}_{2\pi}$, hence $a = -6$ and $b = 1$. The respective angles of rotation and lengths of translation of the related helical displacements are

$$\boldsymbol{l} = (-54.231^\circ,\ 3.6456),\ \ \boldsymbol{r} = (34.614^\circ,\ 21.8738).$$

The basic quadrangle $V_1 \ldots V_4$ has the interior angles 70.0° at V_1, 50.0° at V_2, 160.0° at V_3, and 80.0° at V_4. The side lengths are $V_1V_2 = 25.0$, $V_2V_3 = 13.7416$, $V_3V_4 = 11.7705$, and

[6] When in the sequel faces f_{ij} with $i > m$ or $j > n$ show up then they belong to extensions of our $m \times n$ tessellation mesh.

[7] In this context a negative n means for the column index j of the faces f_{ij}: $j = 1, 0, -1, \ldots, n\,.$

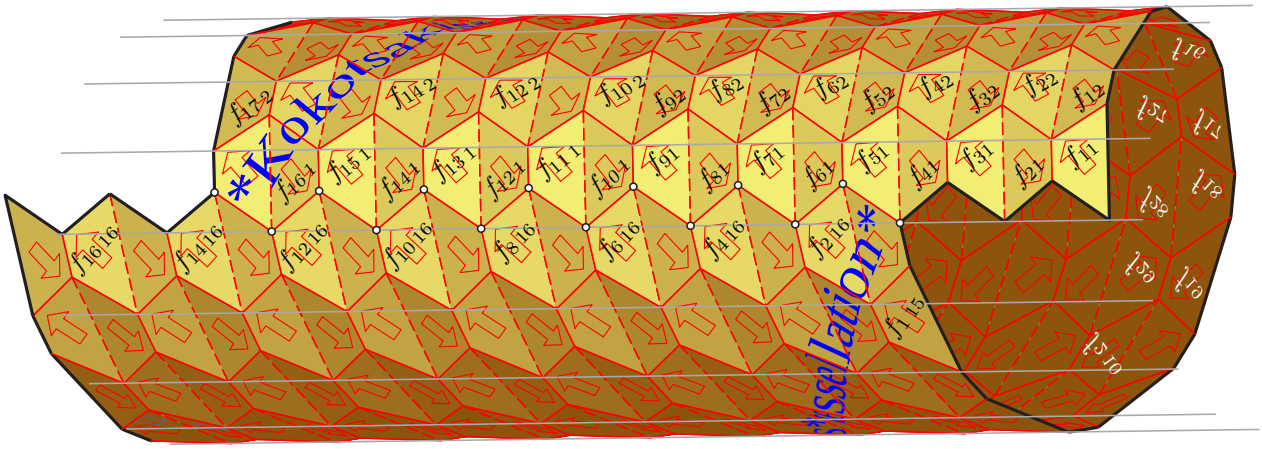

Figure 14: A basic trapezoid yields a modified Schwarz lantern (or Schwarz boot)

$V_4V_1 = 17.4653$. The dihedral angles of the depicted flexion are at V_1V_2 205.052° (valley fold), at V_4V_1 145.731°, at V_2V_3 112.759°, and at V_3V_4 143.029°.
The flexion bounds a solid. It can be produced by Boolean operations from the solid cylinder of revolution $\mathcal{C}$ passing through the vertices as follows: We start with two faces sharing a valley fold (indicated by dashes in the figures). The exterior half spaces of the spans of these two faces intersect in a wedge $\mathcal{W}$. Now we subtract from the solid cylinder $\mathcal{C}$ all wedges which arise from $\mathcal{W}$ by iterated helical displacements $\boldsymbol{r}$ and $\boldsymbol{l}$.

Example 2. In Fig. 14 the basic quadrangle is an unsymmetric trapezoid. The displayed flexion can be seen as generalized *Schwarz lantern* or *Schwarz boot:* The original Schwarz lantern ('diamond pattern' in origami) is a triangular mesh approximating a cylindrical surface. The German mathematician Hermann Amandus Schwarz (1843-1921) could prove that depending on the refinement of this mesh the discrete area either converges towards the surface area of the cylinder or tends to infinity.
We notice at the 17×16 TM in Fig. 14 that according to Theorem 4 sequences of vertices are placed on generators of the cylinder.

Data: The basic trapezoid has the side lengths $V_1V_2 = 20.0$, $V_2V_3 = 12.9332$, $V_3V_4 = 7.0668$, and $V_4V_1 = 10.9316$. The interior angles at $V_1, \ldots, V_4$ are 65.0°, 50.0°, 130.0° and 115.0°. The bending angle at edge V_1V_2 is 194.6615° (valley fold), at V_2V_3 151.0106°, at V_3V_4 165.3385°, and at V_4V_1 155.5731°. The respective angles of rotation and lengths of translation of the generating helical displacements are

$$\boldsymbol{l} = (-22.5°,\ 7.49883),\quad \boldsymbol{r} = (22.5°,\ 12.49804).$$

We have $(n, k) = (16, 4)$, $(a, b) = (-10, 6)$ and we can confirm $-10 \cdot 7.49883 + 6 \cdot 12.49804 = 0$ and $-10 \cdot (-22.5) + 6 \cdot 22.5 = 360.0$.

3.3. Another approach to closing flexions

There is an alternative approach to tessellation meshes with a horizontally closing flexion: We start with half-turns $\boldsymbol{\rho}_1, \ldots, \boldsymbol{\rho}_4$ such that by (2) the corresponding $\boldsymbol{r}$ and $\boldsymbol{l}$ obey Theorem 7.

First we specify an appropriate cartesian coordinate frame: The x-axis is the axis of the half-turn $\boldsymbol{\rho}_1$, the z-axis coincides with the helical axis p. Let (r, φ, z) denote the corresponding cylinder coordinates with $x = r\cos\varphi$, $y = r\sin\varphi$.

We set up the respective cylinder coordinates of the axes of $\boldsymbol{\rho}_1, \boldsymbol{\rho}_2, \boldsymbol{\rho}_4$ by

$$(\mathbb{R},\, 0,\, 0), \quad \left(\mathbb{R},\, \frac{\sigma}{2},\, \frac{s}{2}\right), \quad \left(\mathbb{R},\, \frac{\tau}{2},\, \frac{t}{2}\right).$$

Then we obtain a representation of these half-turns and by (1) of $\boldsymbol{\rho}_3 = \boldsymbol{\rho}_2\boldsymbol{\rho}_1\boldsymbol{\rho}_4$ in cylinder coordinates:

$$\begin{array}{ll} \boldsymbol{\rho}_1\colon\ (r,\varphi,z) \mapsto (r,\, -\varphi,\, -z) & \\ \boldsymbol{\rho}_2\colon\ (r,\varphi,z) \mapsto (r,\, -\varphi+\sigma,\, -z+s) & \boldsymbol{l}\colon\ (r,\varphi,z) \mapsto (r,\, \varphi+\tau,\, z+t) \\ \boldsymbol{\rho}_3\colon\ (r,\varphi,z) \mapsto (r,\, -\varphi+\sigma+\tau,\, -z+s+t) & \boldsymbol{r}\colon\ (r,\varphi,z) \mapsto (r,\, \varphi+\sigma,\, z+s) \\ \boldsymbol{\rho}_4\colon\ (r,\varphi,z) \mapsto (r,\, -\varphi+\tau,\, -z+t) & \end{array} \tag{9}$$

The closure conditions given in Theorem 7 are equivalent to

$$a\tau + b\sigma = 2\pi, \quad at + bs = 0 \ \text{ for } \ a, b \in \mathbb{Z}. \tag{10}$$

By (5) we obtain for any arbitrary vertex V_1 the other vertices of the face f_{22} (see Fig. 2 or 7). The vertices of $f_{11} = \boldsymbol{r}^{-1}(f_{22})$ are

$$\begin{aligned} \boldsymbol{r}^{-1}(V_3) &= V_1 = (r,\, \varphi,\, z), \\ \boldsymbol{r}^{-1}(V_2) &= \boldsymbol{\rho}_1(V_1) = (r,\, -\varphi,\, -z), \\ \boldsymbol{r}^{-1}(V_1) &= (r,\, \varphi-\sigma,\, z-s), \\ \boldsymbol{r}^{-1}(V_4) &= \boldsymbol{\rho}_4(V_1) = (r,\, -\varphi+\tau,\, -z+t). \end{aligned}$$

However, this implies a condition on V_1: The planarity of this quadrangle is equivalent to

$$\det \begin{pmatrix} 1 & x & y & z \\ 1 & x & -y & -z \\ 1 & x\cos\sigma + y\sin\sigma & y\cos\sigma - x\sin\sigma & z-s \\ 1 & x\cos\tau + y\sin\tau & x\sin\tau - y\cos\tau & t-z \end{pmatrix} = 0.$$

After some computation we obtain from the determinant the polynomial

$$\begin{aligned} &P(x,y,z) := [t(\cos\sigma - 1) + s(\cos\tau - 1)]\, xy + (t\sin\sigma + s\sin\tau)\, y^2 \\ &+ 2\,[\cos(\sigma+\tau) - \cos\sigma - \cos\tau + 1]\, xyz + [\sin(\sigma+\tau) - \sin\sigma - \sin\tau]\, (y^2 - x^2)z. \end{aligned} \tag{11}$$

The zero set of P is a ruled surface of degree 3 with the cylinder axis p ($= z$-axis) as double line and with generators orthogonal to p. For geometrical reasons this cubic surface passes through the axes of the half-turns $\boldsymbol{\rho}_1$ and $\boldsymbol{\rho}_4$.

For a cylinder tessellation with planar quadrangles it is necessary that besides (10) vertex V_1 is a point of the cubic surface $P = 0$. In addition, we have to check whether the quadrangle $V_1 \ldots V_4$ is convex. When V_1 is specified on the axis of $\boldsymbol{\rho}_1$ we obtain a triangle since two vertices coincide; of course, a triangle is convex. Hence a small variation of V_1 on the cubic surface gives a planar quadrangle $V_1\ \boldsymbol{\rho}_1(V_1)\ \boldsymbol{r}^{-1}(V_1)\ \boldsymbol{\rho}_4(V_1)$ which is either convex or has a self-intersection. In the latter case we choose V_1 sufficiently close to the previous $\boldsymbol{\rho}_1(V_1)$ in order to obtain convexity. The same holds for V_1 in the neighbourhood of the axis of $\boldsymbol{\rho}_4$.

Theorem 8. *When the axes of $\boldsymbol{\rho}_1, \ldots, \boldsymbol{\rho}_4$ are given with a common perpendicular p and obeying (1) as well as Theorem 7, then there is a two-parameter set of planar convex quadrangles which define horizontally closing tessellation meshes.*

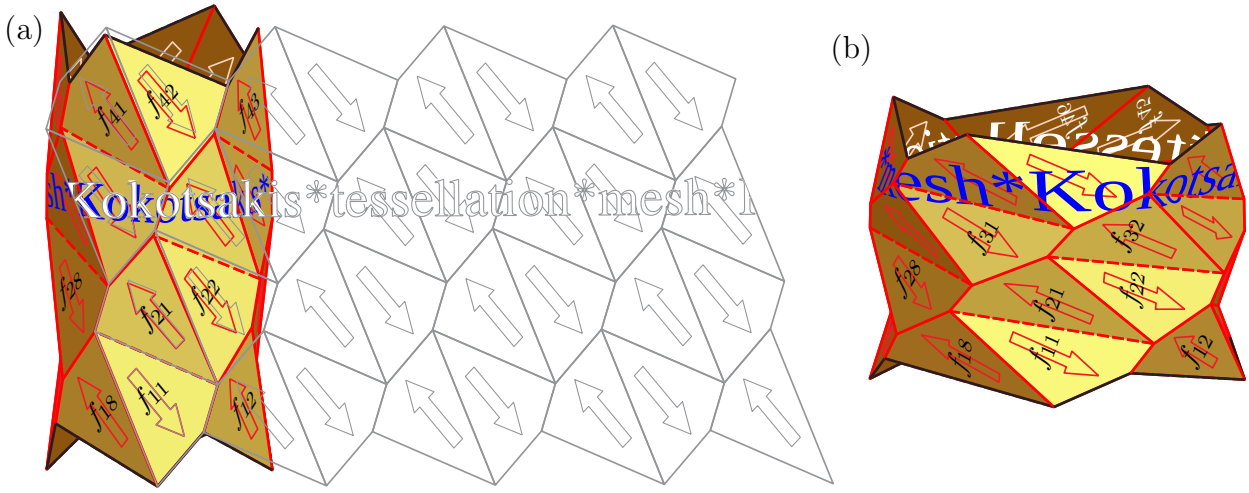

Figure 15: Two 4×8 tessellations with rotational symmetry ($k = 0$), see Example 3. The flexion (b) arises from (a) by an axial dilatation.

Example 3. In Fig. 15 two horizontally closing flexions of 4×8 TMs with vertical shift $k = 0$ are displayed. This implies $a = -\frac{n+k}{2} = -4$ and $b = \frac{n-k}{2} = 4$. The data defining the helical displacements $\boldsymbol{r}$ and $\boldsymbol{l}$ are as follows: In both cases we have $\sigma = 32.0°$ and $\tau = -58.0°$. The angle of rotation for the vertical shift $\boldsymbol{lr}$ is $\sigma + \tau = -26°$. In the left hand figure (a) we have $s = t = 35.293$, in (b) $s = t = 17.805$.

The flexion (b) arises from (a) by an *axial dilation* which preserves the rotational symmetry about the cylinder axis p thus underlining that the radius r plays no role in Eq. (11) . Despite of this close relation between these two flexions the dimensions of the underlying quadrangles and the bending angles are totally different:

The quadrangle $V_1 \dots V_4$ of (a) has the interior angles 62.479°, 156.031°, 97.034°, 44.456°, and the side lengths $V_1V_2 = 25.000$, $V_2V_3 = 17.424$, $V_3V_4 = 47.148$, and $V_4V_1 = 58.840$. The respective dihedral angles along these edges are 155.086°, 126.757°, 197.868° (valley fold), and 137.674°.

In (b) the interior angles are 112.143°, 152.072°, 61.577°, 34.208°, the side lengths $V_1V_2 = 25.000$, $V_2V_3 = 11.389$, $V_3V_4 = 61.344$, and $V_4V_1 = 42.456$. The corresponding bending angles are 132.705°, 113.998°, 224.137° (valley fold), and 122.053°.

Example 4. Figure 16 shows a flexion of a 3×18 TM wrapped without gaps around a cylinder. The first nine columns determine a horizontally closing flexion with vertical shift $k = -3$. Note that this crease ribbon only admits a one-parameter self-motion; once a single bending angle is fixed, the flexion of the whole TM is uniquely determined. Hence, the ribbon cannot be wrapped around the cylinder sequentially like a tape.

The base quadrangle $V_1 \dots V_4$ has the interior angles 26.588°, 133.692°, 132.893°, 66.827°, and the side lengths $V_1V_2 = 35.0$, $V_2V_3 = 17.272$, $V_3V_4 = 10.700$, and $V_4V_1 = 51.769$. The respective dihedral angles along these edges are 193.209° (valley fold), 133.866°, 139.599°, and 170.854°.

The angles of rotation and lengths of translation of the related helical displacements

$$\boldsymbol{l} = (-50.40°,\ 45.290), \quad \boldsymbol{r} = (34.80°,\ 22.645).$$

fulfill the conditions of Theorem 7 with $a = -3$ and $b = 6$.

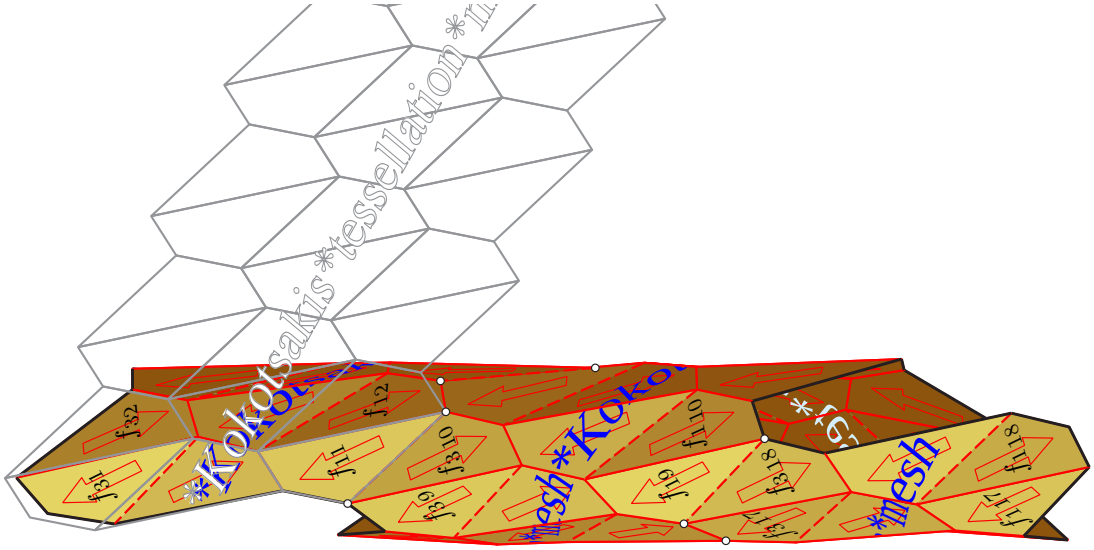

Figure 16: A 3×18 tessellation mesh with a flexion tiling the cylinder (Example 4)
The marked points indicate the border line between consecutive windings.

3.4. On the rigidity of a closing flexion

We learned that non-trivial flexions of tessellation meshes are either isolated or poses obtained during a one-parameter self-motion. Therefore one can expect that in the case of a horizontally closing flexion the constraint of attaching the right border line to the left one restricts the flexibility. We can even state:

Theorem 9. *Let a horizontally closing non-trivial flexion of a $m \times n$ tessellation mesh be given with $m, n \geq 3$ and with vertical shift k obeying $-n \leq k \leq n$. When the right and the left border line are glued together at least at one vertex, then in the case of non-cyclic base quadrangles the resulting quad mesh is infinitesimally rigid.*

Proof: Under the restriction $-n \leq k \leq n$ there is an overlap of at least one vertex between the left and the right border zig-zag. We must prove that the only infinitesimal motion, which the quad mesh with one pair of glued vertices can perform, is the trivial one.

For this purpose we keep face f_{11} fixed and assume that in our flexion (in the sense of Footnote 6) f_{11} coincides by Theorem 7 with $f_{1-k\,1+m}$. Now we confirm on the basis of *screw-theory* that there is no non-trivial infinitesimal motion of our quad mesh such that any vertex of $f_{1-k\,1+m}$ obtains a zero-velocity.

Any infinitesimal motion of our TM assigns to each face f_{jk} a *twist* (see, e.g., [1] or [6]), i.e., a pair of vectors $(\boldsymbol{q}_{jk}, \boldsymbol{q}_{jk\,0})$ — usually combined to a *dual vector* $\widehat{\boldsymbol{q}}_{jk} = \boldsymbol{q}_{jk} + \varepsilon\, \boldsymbol{q}_{jk\,0}$ obeying $\varepsilon^2 = 0$ — such that for any point $\boldsymbol{x}$ attached to f_{jk} the velocity vector reads

$$\boldsymbol{v}_{\boldsymbol{x}} = \boldsymbol{q}_{jk\,0} + (\boldsymbol{q}_{jk} \times \boldsymbol{x}).$$

Due to the spatial Aronhold-Kennedy-Theorem, for any two faces sharing an edge e the relative motion is a rotation about the common edge with any angular velocity ω. This implies that the difference of the associated twists equals $\omega\, \widehat{\boldsymbol{e}} = \omega(\boldsymbol{e} + \varepsilon\, \boldsymbol{e}_0)$ with $\boldsymbol{e}$ as unit direction vector and $\boldsymbol{e}_0$ as momentum vector of edge e (see, e.g., [6]).

For the primary 2×2 TM with faces f_{11}, f_{12}, f_{21}, and f_{22} the corresponding spherical

four-bar defines the respective twists inclusive $\widehat{\boldsymbol{q}}_{11} = \mathbf{0}$ up to a common real factor.[8] This can be continued step by step to other 2×2 sub-meshes until finally we obtain the twist $\widehat{\boldsymbol{q}}_{1-k\,1+m}$ of the face $f_{1-k\,1+m}$. We will see that the instantaneous motion of this face is again helical with axis p.

For the sake of brevity we prefer a direct way to compute the twist $\widehat{\boldsymbol{q}}_{1-k\,1+m}$. We know by Lemma 5 that for each non-trivial flexion there is a helical motion about an axis p through angle φ and with translational length l which maps f_{11} onto $f_{1-k\,1+m}$. We use a coordinate frame attached to f_{11} and set up p by a unit direction vector $\boldsymbol{d}$ and its point $\boldsymbol{m}$ of intersection with the plane $[f_{11}]$. By Corollary 3 point $\boldsymbol{m}$ is always finite. Of course, when the self-motion is performed, $\boldsymbol{p}$, $\boldsymbol{m}$, φ and l are functions of time u. We may suppose $\dot{\boldsymbol{p}} \neq \mathbf{0}$ due to a regular parametrization of the quadratic director cone (Corollary 3).

The required helical motion mapping a point $\boldsymbol{x} \in f_{11}$ onto a point $\boldsymbol{x}' \in f_{1-k\,1+m}$ can be expressed by

$$\boldsymbol{x}' - \boldsymbol{m} = \cos\varphi(\boldsymbol{x} - \boldsymbol{m}) + \big[(1 - \cos\varphi)\big(\boldsymbol{p} \cdot (\boldsymbol{x} - \boldsymbol{m})\big) + l\,\big]\,\boldsymbol{p} + \sin\varphi\,[\boldsymbol{p} \times (\boldsymbol{x} - \boldsymbol{m})]\,. \tag{12}$$

Differentiation by time u yields for the infinitesimal motion of $f_{1-k\,1+m}$

$$\begin{aligned} \dot{\boldsymbol{x}}' - \dot{\boldsymbol{m}} = \; & -\dot\varphi\,\sin\varphi(\boldsymbol{x} - \boldsymbol{m}) - \cos\varphi\,\dot{\boldsymbol{m}} + \big[\dot\varphi\,\sin\varphi\big(\boldsymbol{p} \cdot (\boldsymbol{x} - \boldsymbol{m})\big) \\ & + (1 - \cos\varphi)\big(\dot{\boldsymbol{p}} \cdot (\boldsymbol{x} - \boldsymbol{m})\big) - (1 - \cos\varphi)(\boldsymbol{p} \cdot \dot{\boldsymbol{m}}) + \dot l\,\big]\boldsymbol{p} \\ & + \big[(1 - \cos\varphi)\big(\boldsymbol{p} \cdot (\boldsymbol{x} - \boldsymbol{m})\big) + l\,\big]\;\dot{\boldsymbol{p}} + \dot\varphi\,\cos\varphi\,[\boldsymbol{p} \times (\boldsymbol{x} - \boldsymbol{m})] \\ & + \sin\varphi\,\big[\big(\dot{\boldsymbol{p}} \times (\boldsymbol{x} - \boldsymbol{m})\big) - \big(\boldsymbol{p} \times \dot{\boldsymbol{m}}\big)\big]\,. \end{aligned} \tag{13}$$

We focus on the pose $u = u_0$ which is horizontally closing, i.e., $\varphi(u_0) = 2\pi$ and $l(u_0) = 0$. Then (13) implies

$$\boldsymbol{v}_{\boldsymbol{x}'} = \dot{\boldsymbol{x}}' = \dot l\,\boldsymbol{p} + \dot\varphi\;[\boldsymbol{p} \times (\boldsymbol{x} - \boldsymbol{m})]\,.$$

Therefore the instantaneous twist of $f_{1-k\,1+m}$ for $u = u_0$ reads

$$\widehat{\boldsymbol{q}}_{1-k\,1+m} = \dot\varphi\,\boldsymbol{p} + \varepsilon\big[\dot l\,\boldsymbol{p} - \dot\varphi\,(\boldsymbol{p} \times \boldsymbol{m})\big] = (\dot\varphi + \varepsilon\,\dot l)\,(\boldsymbol{p} + \varepsilon(\boldsymbol{m} \times \boldsymbol{p})) = (\dot\varphi + \varepsilon\,\dot l)\widehat{\boldsymbol{p}}\,. \tag{14}$$

The instantaneous motion of $f_{1-k\,1+m}$ is a helical motion about axis p with angular velocity $\dot\varphi$ and translational velocity $\dot l$. In the case $\dot l = 0$, $\dot\varphi \neq 0$ point $\boldsymbol{m}$ is fixed, but by Corollary 3 point $\boldsymbol{m}$ never coincides with one vertex of $f_{1-k\,1+m}$. Only under $\dot\varphi = \dot l = 0$ there exists a fixed vertex; the face $f_{1-k\,1+m}$ has a stillstand. However, we prove in the sequel that $\dot l = 0$ for $u = u_0$ leads to a contradiction:

By Lemma 5 and Theorem 7 we have $a, b \in \mathbb{Z} \setminus \{(0,0)\}$ with $\varphi = a\tau + b\sigma$ and $l = at + bs$ where by (9) the pairs (τ, t) and (σ, s) denote the angles of rotation and lengths of translation of $\boldsymbol{l}$ and $\boldsymbol{r}$, respectively. When the vertices of f_{11} have coordinate vectors $\boldsymbol{v}_1, \ldots, \boldsymbol{v}_4$, then $s = (\boldsymbol{v}_3 - \boldsymbol{v}_1) \cdot \boldsymbol{p}$ and $t = (\boldsymbol{v}_4 - \boldsymbol{v}_2) \cdot \boldsymbol{p}$ (compare Fig. 2). This implies $\dot l = a\dot t + b\dot s$ with $\dot s = (\boldsymbol{v}_3 - \boldsymbol{v}_1) \cdot \dot{\boldsymbol{p}}$ and $\dot t = (\boldsymbol{v}_4 - \boldsymbol{v}_2) \cdot \dot{\boldsymbol{p}}$. Hence, $l = \dot l = 0$ for $u = u_0$ results in

$$\boldsymbol{n} \cdot \boldsymbol{p} = \boldsymbol{n} \cdot \dot{\boldsymbol{p}} = 0 \;\; \text{for} \;\; \boldsymbol{n} := a(\boldsymbol{v}_4 - \boldsymbol{v}_2) + b(\boldsymbol{v}_3 - \boldsymbol{v}_1) \neq \mathbf{0}\,. \tag{15}$$

The linearly independent vectors $\boldsymbol{p}$ and $\dot{\boldsymbol{p}}$ span a tangent plane of the quadratic director cone of cylinder axes, and this plane is orthogonal to the vector $\boldsymbol{n}$ which — as a linear combination

[8] Only for a trivial flexion in the trapezoidal case the space of infinitesimal motions is two-dimensional since the spherical four-bar consists of two half-circles (note page 159).

of the two diagonal vectors of f_{11} — lies in a symmetry plane of the cone. Hence for a non-degenerate cone, i.e., for a non-cyclic base quadrangle, $\boldsymbol{p}(u_0)$ must be a direction vector of one of the generators in the symmetry plane parallel $[f_{11}]$, but by Corollary 3 these generators are no more axes of cylinders of rotation through the base quadrangle. □

Remark: It remains open whether in the case of a cyclic quadrangle $V_1, \ldots, V_4$ the necessary and sufficient conditions $a\tau + b\sigma = 2\pi$, $a\dot{\tau} + b\dot{\sigma} = at + bs = a\dot{t} + b\dot{s} = 0$ for infinitesimal flexibility of a non-flat horizontally closing TM can simultaneously be fulfilled. Note that because of the splitting director cone the vector $\boldsymbol{n}$ defined in (15) must bisect the angle between the diagonals in f_{11}.

4. Conclusions

We studied flexions of the planar tessellation with congruent convex quadrangles. Under the conditions given in Theorem 7 there are flexions which tile a cylinder. This offers a possibility to build rigid discrete models of cylinders of revolution from congruent planar convex quadrangles. One can find the dimensions of such cylinder tilings either numerically by an appropriate algorithm or by starting with a pair of coaxial helical motions $\boldsymbol{r}$, $\boldsymbol{l}$ obeying Eq. (10) and specifying one vertex on a cubic surface.

Acknowledgments

This research is supported by Grant No. I 408-N13 of the Austrian Science Fund FWF within the project "Flexible polyhedra and frameworks in different spaces", an international cooperation between FWF and RFBR, the Russian Foundation for Basic Research.

References

[1] J. Angeles: *Fundamentals of robotic mechanical systems*. Springer, New York 2007.

[2] A.I. Bobenko, T. Hoffmann, W.K. Schief: *On the Integrability of Infinitesimal and Finite Deformations of Polyhedral Surfaces*. In A.I. Bobenko et al. (eds.): *Discrete Differential Geometry*. Oberwolfach Seminars **38**, 67–93 (2008).

[3] C.S. Borcea, I. Streinu: *Periodic frameworks and flexibility*. Proc. R. Soc. A 8 **466**, no. 2121, 2633–2649 (2010).

[4] A. Kokotsakis: *Über bewegliche Polyeder*. Math. Ann. **107**, 627–647 (1932).

[5] H. Schaal: *Konstruktion der Drehzylinder durch vier Punkte einer Ebene*. Sitzungsber., Abt. II, österr. Akad. Wiss., Math.-Naturw. Kl. **195**, 405–418 (1986).

[6] H. Stachel: *Teaching Spatial Kinematics for Mechanical Engineering Students*. Proceedings 5th Aplimat 2006, Bratislava/Slovak Republic, Part I, pp. 201–209.

[7] H. Stachel: *A kinematic approach to Kokotsakis meshes*. Comput. Aided Geom. Des. **27**, 428–437 (2010).

[8] H. Stachel: *Remarks on flexible quad meshes*. Proc. 11th Internat. Conference on Engineering Graphics — Baltgraf-11, Tallinn/Estonia, pp. 84–92.

[9] H. Stachel: *On the Rigidity of Polygonal Meshes*. South Bohemia Mathematical Letters **19** (1), 6–17 (2011).

Received August 2, 2012; final form December 9, 2012